JOURNAL OF IRON AND STEEL RESEARCH, INTERNATIONAL. 2008, 15(1): 79-84

Influence of Lanthanum Ion-Implantation on Adhesive Property of Oxide Film Formed on Co-40Cr Alloy

JIN Hui-ming[1], ZHANG Lin-nan[2], LIU Xiao-jun[2]
(1. Yangzhou University, Yangzhou 225009, Jiangsu, China; 2. Northeastern University, Shenyang 110025, Liaoning, China)

Abstract: The isothermal and cyclic oxidizing kinetics of Co-40Cr alloy and its lanthanum ion-implanted samples were studied at 1 000 ℃ in air by thermal gravimetric analysis (TGA). Scanning electron microscopy (SEM) was used to examine the Cr_2O_3 oxide film's morphology after oxidation. Secondary ion mass spectrum (SIMS) method was used to examine the binding energy change of chromium caused by La-doping and its influence on the formation of Cr_2O_3 film. Acoustic emission (AE) method was used in situ to monitor the cracking and spalling of oxide films during oxidizing and subsequent air-cooling stages. Laser Raman spectrum was used to examine the stress changes within oxide films. A theoretical model was proposed relating to the film fracture process and was used to analyze the AE spectrum both on time domain and AE-event number domain. It was found that lanthanum implantation remarkably reduced the isothermal oxidizing rate of Co-40Cr and improved the anti-cracking and anti-spalling properties of Cr_2O_3 oxide film. The reasons for the improvement were mainly that the implanted lanthanum reduced the grain size and internal stress of Cr_2O_3 oxide, increased the high temperature plasticity of oxide film, and remarkably reduced the number and size of Cr_2O_3/Co-40Cr interfacial defects.

Key words: oxidation; adhesion; acoustic emission; laser Raman; lanthanum

The resistance of high-temperature alloys to the oxidizing environment depended on the formation of slow-growing and adherent oxide films. Usually there are intrinsic growing stress and external thermal stress formed in oxide films[1,2]. The former might arise from the volume changes when the metal is oxidized to oxide, whereas the latter might arise from the thermal expansion difference between the metal and the oxides. Many studies[1-8] had been carried out relating to the isothermal and cyclic oxidation behaviors of different super-alloys and high temperature coatings. In this study, acoustic emission (AE) method was used to monitor the cracking and spalling of oxide film formed on Co-40Cr alloy during high-temperature oxidation. A related mechanical and mathematical model was proposed to study the Cr_2O_3/Co-40Cr interfacial defects' distribution, and finally the influence of lanthanum ion-implantation on the high temperature oxidation of Co-40Cr was evaluated by this method and other oxide structure analyzing methods.

1 Experimental Methods

Co-40Cr alloy was cut by wire-electrode cutting into 10 mm×10 mm×1 mm samples which were ultimately polished using a 0.2 μm Al_2O_3 abrasive paste. After being ultrasonically cleaned in acetone and alcohol solution, some specimens were implanted by 3×10^{17} La^+/cm^2 using MEVVE-8010 ion-implantation machine. Isothermal oxidation and cyclic oxidation (55 min heating +5 min air-cooling) were carried out at 1 000 ℃ in air in M25DV thermal balance to study the oxidation kinetics of Co-40Cr and La-implanted Co-40Cr alloy. Scanning electron microscopy (SEM) was used to examine the surface morphology of oxide films. Secondary ion mass spectrum (SIMS) technique was used to analyze the lanthanum depth profile in substrate Co-40Cr before oxidation and in Cr_2O_3 oxide film after oxidation, respectively. SIMS technique was also used to measure the binding energy changes of

Foundation Item: Item Sponsored by National Natural Science Foundation of China (59231011)
Biography: JIN Hui-ming(1968-), Male, Doctor, Professor; **E-mail**: doctorjhm@sohu.com; **Revised Date**: December 5, 2005

element Cr caused by La-implantation. Laser Raman spectrum was used to examine the internal stress changes within oxide films.

2 Results and Discussion

The isothermal oxidation mass-gain curves of Co-40Cr and Y-implanted Co-40Cr are shown in Fig. 1. It can be seen that the lanthanum implantation remarkably reduced the oxidizing rate of Co-40Cr alloy. Cyclic oxidation mass change curves of Co-40Cr and La-implanted Co-40Cr are shown in Fig. 2, in which one can observe that severe oxide spallation (i. e. , mass loss) occurred in La-free Co-40Cr after 20 h cyclic oxidation, whereas La-doped Co-40Cr showed no obvious spallation during the 90 h cyclic oxidation stage.

Fig. 3 illustrates the SEM morphologies of the oxide films formed on Co-40Cr and its La-implanted samples after 24 h isothermal oxidation. One can find that lanthanum ion-implantation remarkably reduced the grain size of oxide film, and ridge character had apparently arisen in the La-containing oxide film [Fig. 3 (b)]. Energy dispersive spectrum (EDS)

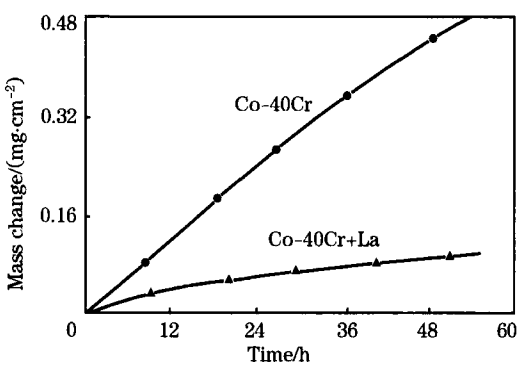

Fig. 1 Isothermal oxidizing mass-gain curves of Co-40Cr and La-implanted Co-40Cr

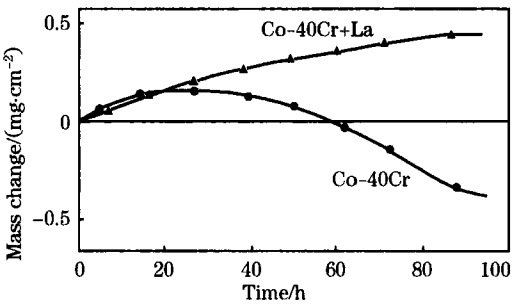

Fig. 2 Cyclic oxidation mass change curves of Co-40Cr and La-implanted Co-40Cr

analysis showed that the oxide films formed on two kinds of samples were both pure Cr_2O_3, because of the high Cr content and its preferential oxidation in Co-Cr binary alloy[4].

The maximum depth of ion-implantation is usually less than 100 nm and it would introduce large amounts of dislocation in the alloy surface[2,3]. During the initial oxidizing stage, the implanted lanthanum with high local concentration and high chemical activity would act as the Cr_2O_3 crystal-forming site and promote fine-grained Cr_2O_3 oxide formation[2].

In SIMS experiment, when the sample surface was bombarded by first Ar^+ ion, the kinetic energy of the first Ar^+ ion (E_P) was equal to the total of secondary ion's kinetic energy (E_K), element-binding energy (E_B) and energy loss (E_L). During the experiment, E_P was kept at a constant value and E_L was regarded as unchangeable[4]. Hence, the binding energy change for an element was

$$\Delta E_B = -\Delta E_K = -e\Delta U_R \quad (1)$$

where ΔU_R was the retarding voltage change which could be obtained by extrapolating the liner part of the secondary ion intensity curves to U_R abscissa as shown in Fig. 4.

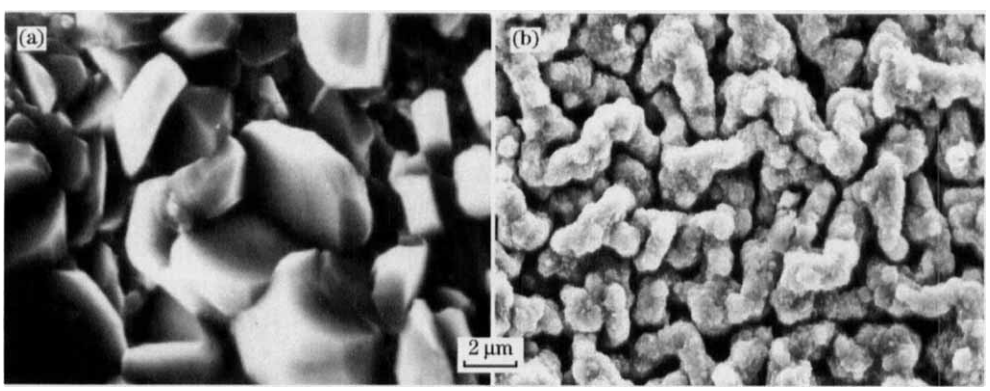

Fig. 3 SEM morphologies of oxide films formed on Co-40Cr (a) and La-implanted Co-40Cr (b) after 24 h isothermal oxidation

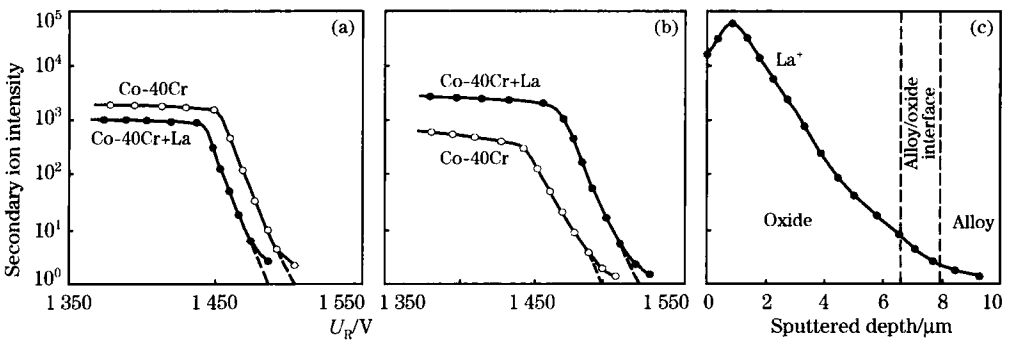

Fig. 4 Secondary Cr^{3+} ion intensity curves of Co-40Cr and La-implanted Co-40Cr before (a) and after (b) oxidation, and La depth profile along cross section (c)

Fig. 4 (a) shows the chromium secondary ion intensity curve of La-free and La-implanted Co-40Cr before oxidation, and Fig. 4 (b) indicates the chromium secondary ion intensity curve of two kinds of samples after 1 h isothermal oxidation. Fig. 4 (c) depicts the lanthanum depth profile along oxide/substrate cross section after 10 h isothermal oxidation, in which the position of the oxide/alloy interface was determined by detecting secondary Co^{2+} ion intensity changes during the Ar^+ sputtering process.

It could be found that the La-implantation reduced Cr binding energy before oxidation [Fig. 4 (a)]. This effect meant that lanthanum could probably increase Cr_2O_3 crystal formation rate and finally refine Cr_2O_3 oxide grain size[2,8]. In addition, lanthanum would inhibit [Cr^{3+}] ion diffusion within Cr_2O_3 oxide film, which could be confirmed by the Cr-binding energy increase after some long-time oxidation, e. g. , 1 h in the experiment shown in Fig. 4 (b), and change the oxidizing rate-controlling step from predominant [Cr^{3+}] cation outward diffusion to predominant [O^{2-}] anion inward diffusion. Studies relating to the ionic diffusion within oxide film had been investigated by some researchers[2,4] using O^{16}/O^{18} tracing element experiment. Predominant [Cr^{3+}] cation's outward diffusion was inhibited. This could partially be confirmed by SIMS experiment, in which lanthanum's final position after 10 h oxidation was located near the outer surface of Cr_2O_3 oxide film as shown in Fig. 4 (c).

In AE experiment, La-free and La-containing specimens were isothermally oxidized at 1 000 ℃ in air for 90 h and then air-cooled to room temperature. During the 90 h isothermal oxidizing stage almost no AE signal was detected, whereas in the air-cooling stage many AE signals were detected as shown in Fig. 5.

During the isothermal oxidizing stage, the growth stress σ_{gw} was caused by volume change when the metal was oxidized to its oxide, which could be quantitatively correlated to Pilling-Bedworth ratio (PBR) (volume of oxide/volume of metal

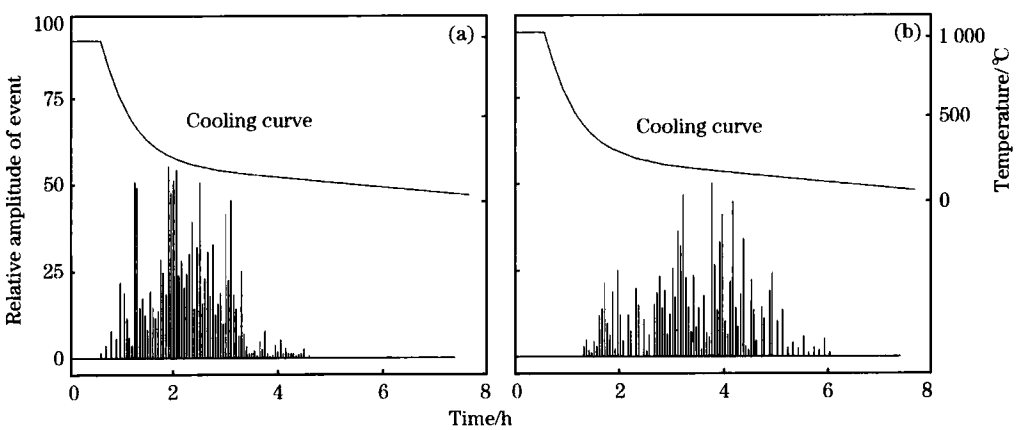

Fig. 5 AE signal distributions measured in air-cooling stage after 90 h isothermal oxidation of Co-40Cr (a) and La-implanted Co-40Cr (b)

consumed). For chromium, this value was 1.57 and the internal growth stress within the Cr_2O_3 oxide film was compressive[2,9].

During the air-cooling stage, thermal stress was generated because of the linear thermal expansion difference between Cr_2O_3 and substrate metal. This thermal stress σ_{th} was also compressive and could be expressed as

$$\sigma_{th}=\frac{E_{OX}\Delta T(\alpha_M-\alpha_{OX})}{1-v} \tag{2}$$

where E_{OX} is the Young's modulus of the oxide; v the Poisson's ratio of the oxide; α_M and α_{OX} are the thermal expansion coefficient of the metal and oxide, respectively; and ΔT is the temperature change. Therefore, the total compressive stress σ_{OX} in the oxide film can be expressed as

$$\sigma_{OX}=\sigma_{gw}+\frac{E_{OX}\Delta T(\alpha_M-\alpha_{OX})}{1-v} \tag{3}$$

In most cases, the first term in the right side of Eqn. (3) is much smaller than the second term, and can be omitted[2]. This can also be experimentally confirmed by AE test as shown in Fig. 5 that rare AE signal was detected during the 90 h isothermal oxidizing stage and a number of AE signals were detected during the air-cooling stage.

The number of AE signals detected in the oxidizing stage and air-cooling stage can be expressed in a function of temperature change as, $n=f(\Delta T)$, in which n is the number of AE signals collected in a given time interval. According to Zhang's simplification[6], the spalling of oxide above one interfacial defect can generate Z AE events, of which $Z-1$ is from through-thickness cracking along the perimeter of the buckled oxide and 1 from the final spalling, and usually Z is an integer between 5 and 8. Then the number of interfacial defects in a given ΔT interval can be expressed as

$$N=\frac{n}{Z}=\frac{f(\Delta T)}{Z} \tag{4}$$

According to Evans[1], the oxide film spalling process should be preceded by film-buckling process above an interfacial defect. When the accumulative compressive stress inside the oxide film reaches a critical value, oxide film buckling would occur above interfacial defects. The compressive stress in the buckled region was partially relieved, whereas the concentrated stress at the perimeter of this region would cause propagation of crack tip towards the outer face of oxide film, and finally result in through-thickness cracking and spalling of oxide film. The quantitative description for the critical stress condition can be expressed as

$$\sigma_{OX}=\frac{3.6H^2E_{OX}^2}{C^2} \tag{5}$$

where H is the thickness of oxide film and C the radius of interfacial defect (i.e., radius of the local spalled region). This equation implies that each interfacial defect with different radius would spall at different compressive stress level. Because compressive thermal stress was accumulated gradually in the oxide film with increasing the ΔT drop during the air-cooling stage, local oxide upon large interfacial defect would crack and spall at small ΔT drop, whereas oxide upon small interfacial defect would crack and spall at large ΔT drop. This could also be experimentally confirmed from the AE signal spectrum as shown in Fig. 5.

By combining Eqn. (3), Eqn. (4) and Eqn. (5) and by omitting σ_{gw}, Eqn. (6) and Eqn. (7) were obtained:

$$C=1.9H\left[\frac{E_{OX}(1-v)}{\Delta T(\alpha_M-\alpha_{OX})}\right]^{1/2} \tag{6}$$

$$N=\frac{1}{Z}f\left[3.6\frac{E_{OX}H^2(1-v)}{C^2(\alpha_M-\alpha_{OX})}\right] \tag{7}$$

The Young's modulus E_{OX} and Poisson's ratio v for Cr_2O_3 oxide were 153 GPa and 0.32, respectively, liner thermal expansion coefficient α_M and α_{OX} for Co-40Cr and Cr_2O_3 were 0.14 K^{-1} and 0.026 K^{-1} respectively[2,6] (all the above data were the average taken at 750 ℃).

By converting the measured distribution of AE signals in time domain to temperature domain using Hi-Draw2.1 software in AE-100 AE apparatus and by differential calculation of number of AE signals on temperature domain using Eqn. (6) and Eqn. (7), the interfacial defect number distribution (N) *vs* defect size (i.e., radius C) was finally obtained (as shown in Fig. 6).

From Fig. 6 it can be seen that the interfacial defects' number distribution *vs* defect size was roughly

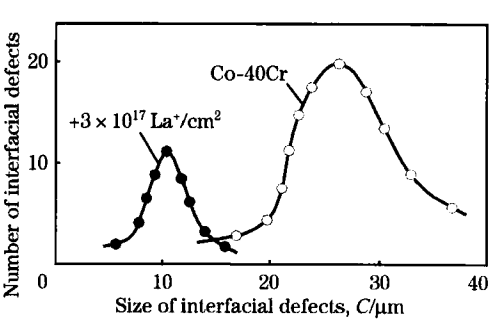

Fig. 6 Number distribution of interfacial defects *vs* defect sizes

expressed by law of Gauss' distribution, and the average interfacial defect radius for Co-40Cr and Y-implanted Co-40Cr were 27.0 μm and 10.5 μm, respectively. Meanwhile lanthanum implantation greatly reduced the total number of interfacial defects, which can be seen by comparing the areas under the two distributional curves in Fig. 6.

Laser Raman technique was used to examine the internal stress changes caused by lanthanum implantation as shown in Fig. 7.

According to Birnie's work[10], mono-chromatic laser light is inelastically scattered to give a Raman spectrum corresponding to a particular molecular and lattice vibrations of solid. When a sample is stressed, the vibration frequencies of the Raman peaks shift to higher frequency for a compressive stress and to lower frequency for a tensile stress. Hence, it can be used in stress measurement and there is a linear relationship between the stress value and its Raman wave-number shift[11]. From Fig. 7 it can be seen that La-implantation reduced the internal compressive stress level in Cr_2O_3 oxide film.

The reasons for the improved property of Cr_2O_3 film in anti-cracking and anti-spallation caused by lanthanum ion-implantation can be explained in two aspects.

First, lanthanum implantation greatly reduced the internal compressive stress level in the Cr_2O_3 film and promoted fine-grained Cr_2O_3 oxide formation. This kind of fine-grained oxide film can have better high temperature plasticity and creeping property, which means that Cr_2O_3 oxide film could relieve parts of the internal compressive stress by means of high-temperature creeping rather than by means of cracking and spalling[11,12]. This type of stress relief via oxide's creeping could be experimentally confirmed by the ridge character of La-doped oxide film in Fig. 3 (b).

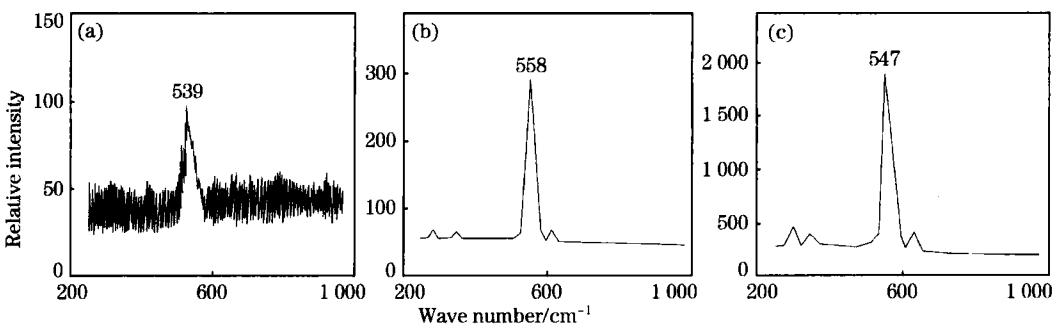

Fig. 7 Raman peaks of standard Cr_2O_3 powder (a), Cr_2O_3 oxides formed on Co-40Cr (b) and La-implanted Co-40Cr (c)

Second, lanthanum implantation remarkably reduced the number and size of the interfacial defects as shown in Fig. 6 and greatly improved the Cr_2O_3/Co-40Cr interfacial adhesive property. Statistic examination of the size of about 100 spalled areas of Y-free and Y-containing Cr_2O_3 oxide films in our experiment by SEM method indicated that the average defect size tested by AE method was about 1.5—2.0 times larger than the SEM-observed average size of the spalled regions. The reason for the higher AE-tested value of the interfacial defect size was probably caused by the interaction between near-existing defects; for the stress relief of one defect would have great influence on the near-located defects' stress status[1,8]. In addition, the choosing of such values as Young's modulus, Poisson's ratio and thermal expansion coefficient of oxide film with different microstructure at different temperature might be another reason for the higher AE-tested average defect size in our experiment[11].

3 Conclusions

(1) Lanthanum ion-implantation remarkably reduced the isothermal oxidizing rate of Co-40Cr at 1 000 ℃; Meanwhile, the anti-cracking and anti-spalling properties of the Cr_2O_3 oxide film were improved very much by La-implantation. These rare earth effects can be mainly attributed to the lower internal stress level, the grain-size refining effect and the improved high-temperature plasticity and creeping property of Cr_2O_3 oxide film.

(2) La-implantation reduced the number and size of oxide/substrate interfacial defects and improved the adhesive property of the oxide film. By using proper mechanical and mathematical methods to simulate the fracture process of oxide film, AE seemed to be a promising method of quantitatively examining oxide/substrate interfacial behaviors.

References:

[1] Evans A G, Cannon R. Stress and Decohesion of Oxide Scales [J]. Materials Science Forum, 1989, 43(3): 243.

[2] Rahmel A, Schutze M. Mechanical Aspects of Rare Earth Effects [J]. Oxidation of Metals, 1992, 38(2): 314.

[3] Hou P U, Stringer J. The Influence of Ion-Implanted Yttrium on the Selective Oxidation of Chromium in Co-25Cr [J]. Oxidation of Metals, 1988, 29(8): 45.

[4] Matychak Y S , Pavlyna V S, Fedirko V M. Kinetics of Selective Oxidation of Chromium Steels in Oxygen Containing Environment [J]. Materials Science, 2003, 39(5): 605.

[5] JIN Hui-ming, ZHANG Jian-feng, YAN Kun. Rare Earth Effects on High Temperature Oxidation of Pure Nickel at 1 000 ℃ [J]. Progress in Natural Science, 2004, 14(4): 373.

[6] ZHANG Yi-fan, Shore D, Rahmel A. Spallation of Oxide Scales Formed on Ni-30Cr Alloy [J]. Oxidation of Metals, 1993, 40(1): 529.

[7] JIN Hui-ming, ZHANG Lin-nan, LI Mei-shuan. Rare Earth Effects on Adhesion of Cr_2O_3 Oxide Scale Formed on Surface of Co-40Cr Alloy [J]. Journal of Rare Earths, 2001, 19(1): 34.

[8] Przybilla W, Schutze M. Role of Growth Stresses on the Structure of Oxide Scales on Nickel at 800 and 900 ℃ [J]. Oxidation of Metals, 2002, 58(1): 103.

[9] Vasyliv B D. Initiation of a Crack From the Edge of a Notch With Oblique Front in Specimens of Brittle Materials [J]. Materials Science, 2002, 38(5): 724.

[10] Birnie J, Cragga C. Ex Situ and in Situ Determination of Stress Distribution in Chromium Oxide Films by Raman Microscopy [J]. Corrosion Science, 1992, 33(2): 1.

[11] JIN Hui-ming, ZHANG Lin-nan, LIU Xiao-jun. Oxidation Mechanism of Magnetically Sputtered Ni-0.5Y Micro-Crystal Coating at 1 000 ℃ [J]. Journal of Iron and Steel Research International, 2004, 11(5): 59.

[12] Ul-Hamid A. Study of the Effect of Y on the Scale Microstructures of Cr_2O_3- and Al_2O_3-Forming Alloys [J]. Oxidation of Metals, 2002, 58(1): 23.